This is an open access article published under an ACS AuthorChoice License, which permits copying and redistribution of the article or any adaptations for non-commercial purposes.

ACS central science

Research Article

Cite This: ACS Cent. Sci. 2018, 4, 97−104

Robust Pinhole-free Li_3N Solid Electrolyte Grown from Molten Lithium

Yanbin Li,[†,#] Yongming Sun,[†,#] Allen Pei,[†] Kaifeng Chen,[‡] Arturas Vailionis,[§] Yuzhang Li,[†] Guangyuan Zheng,[†] Jie Sun,[†] and Yi Cui*[,†,∥]

[†]Department of Materials Science and Engineering, [‡]Department of Applied Physics, and [§]Stanford Nano Shared Facilities, Stanford University, Stanford, California 94305, United States

[∥]Stanford Institute for Materials and Energy Sciences, SLAC National Accelerator Laboratory, 2575 Sand Hill Road, Menlo Park, California 94025, United States

Supporting Information

ABSTRACT: Lithium metal is the ultimate anode choice for high energy density rechargeable lithium batteries. However, it suffers from inferior electrochemical performance and safety issues due to its high reactivity and the growth of lithium dendrites. It has long been desired to develop a materials coating on Li metal, which is pinhole-free, mechanically robust without fracture during Li metal deposition and stripping, and chemically stable against Li metal and liquid electrolytes, all while maintaining adequate ionic conductivity. However, such an ideal material coating has yet to be found. Here we report a novel synthesis method by reacting clean molten lithium foil directly with pure nitrogen gas to generate instantaneously a pinhole-free and ionically conductive α-Li_3N film directly bonded onto Li metal foil. The film consists of highly textured large Li_3N grains (tens of μm) with (001) crystalline planes parallel to the Li metal surface. The bonding between textured grains is strong, resulting in a mechanically robust film which does not crack even when bent to a 0.8 cm curvature radius and is found to maintain pinhole-free coverage during Li metal deposition and stripping. The measured ionic conductivity is up to 5.2×10^{-4} S cm^{-1}, sufficient for maintaining regular current densities for controllable film thicknesses ranging from 2 to 30 μm. This Li_3N coating is chemically stable, isolating the reactive metallic lithium from liquid electrolyte, prevents continuous electrolyte consumption during battery cycling, and promotes dendrite-free uniform lithium plating/stripping underneath. We demonstrated Li|$Li_4Ti_5O_{12}$ cells with stable and flat potential profiles for 500 cycles without capacity decay or an increase in potential hysteresis.

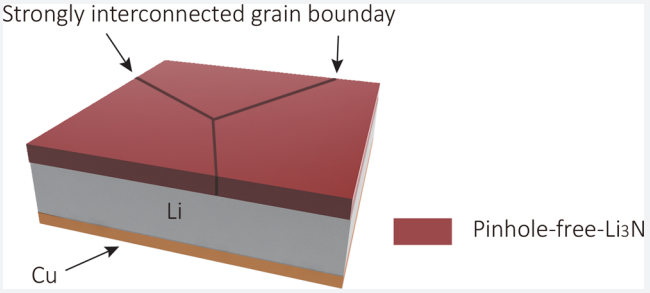

INTRODUCTION

Li metal is the most attractive anode for lithium-based rechargeable batteries because of its high theoretical specific capacity (3861 mAh g^{-1}) and low reduction potential (−3.04 V versus standard hydrogen electrode).[1−4] Although lithium metal has been used in commercialized primary lithium batteries (e.g., Li-MnO_2 battery) featuring high energy density, intrinsic problems such as low Coulombic efficiency, limited cycle life, and safety concerns have long hindered its practical application in rechargeable batteries. To achieve successful Li metal anodes, two fundamental challenges need to be addressed: (1) the highly reactive nature between metallic lithium and liquid electrolytes, and (2) the virtually infinite relative volume change during plating and stripping due to the "hostless" nature of Li metal, resulting in mossy and dendritic Li deposition. During battery charging, liquid electrolytes decompose and react with lithium to form a passivating solid-electrolyte interphase (SEI) on the anode surface.[5] The drastic volume change of Li metal during its stripping and plating processes leads to the significant instability of this SEI. The mechanical fracture of the formed SEI and its repair take place repetitively during battery cycling, resulting in the continuous consumption of liquid electrolytes and lithium, low Coulombic efficiency, large overpotential and short cycle life, ultimately leading to degradation of battery performance.[6] Another challenging problem is the growth of Li dendrites, which form due to current inhomogeneities during battery charging, leading to serious safety problems (Figure 1a).[7,8] Furthermore, when Li is stripped away during battery discharging, some dendrites may break and become electrically isolated from the anode, generating accumulated "dead lithium", which accelerates the degradation of Li batteries and reduces their thermal stability.[9,10]

To make Li metal anodes viable, considerable research effort has been dedicated to understand the process of Li metal plating and stripping,[11−14] and various nanoscale films have been explored for Li metal surface protection, including electrolyte additive derived films,[15−17] atomic layer deposited protection layers (e.g., Al_2O_3),[18] two-dimensional atomic crystal layers (e.g., BN and graphene),[19] hollow carbon hemispheres,[20] in situ

Received: October 7, 2017
Published: December 8, 2017

 © 2017 American Chemical Society

DOI: 10.1021/acscentsci.7b00480
ACS Cent. Sci. 2018, 4, 97−104

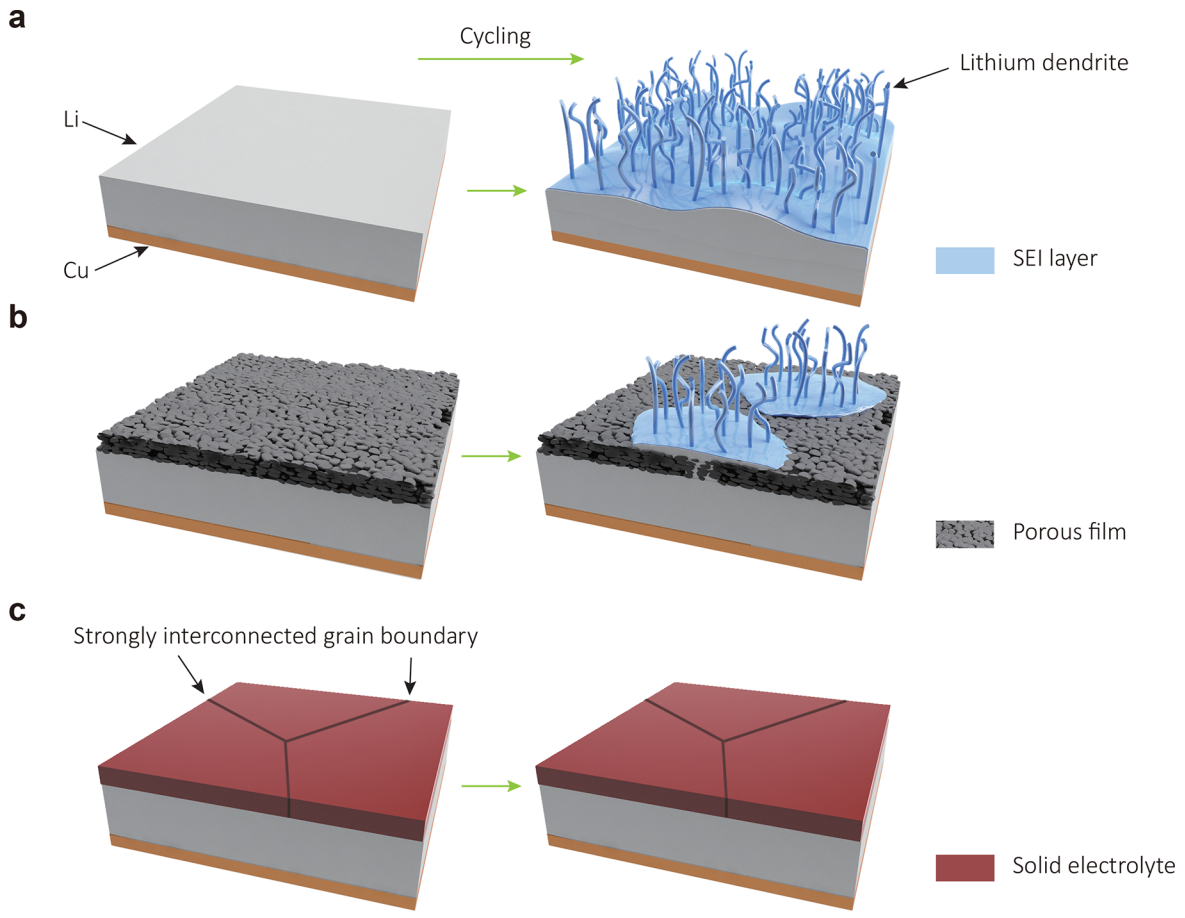

Figure 1. Design and structure of various Li metal anodes. (a) A bare Li metal anode. Upon cycling, Li dendrites grow and liquid electrolytes are rapidly consumed. (b) A nanofilm modified Li metal anode. The pores and/or cracks of the film can trigger growth of Li dendrites and fail in Li metal surface protection. (c) A Li metal anode with a dense, ionically conductive film with strongly interconnected large grains. A dense protective layer with good mechanical durability, high ionic conductivity, and good adhesion to Li metal anodes can isolate Li metal from corrosive liquid electrolytes and enable stable electrochemical stripping and plating of Li metal underneath, preventing dendrite growth and liquid electrolyte consumption.

chemical reaction formed surface films (e.g., Li_3PO_4),[21] conformal lithium fluoride protection layers,[22] and grafted polymer layers.[23] However, despite the great progress, these coated Li metal anodes can still fail during battery fabrication and upon battery cycling due to the insufficient mechanical durability of the nanofilms arising from the weak interconnection between the nanoscale particles. Even with these protective nanofilms, electrolyte can still contact the Li metal directly through pores and cracks, leading to locally enhanced Li ion flux and the growth of Li dendrites (Figure 1b). In this respect, it is highly desirable to have pinhole-free films with large, strongly interconnected grains which can provide better mechanical properties, avoid the undesired side reactions between liquid electrolytes and metallic lithium, and block the formation of Li dendrites, enabling high-performance lithium batteries (Figure 1c). The stable interfacial film would also help stabilizing the three-dimensional host of Li metal recently demonstrated with hollow carbon spheres,[24] graphene oxide,[25] and nanofibers.[26] Li_3N is an excellent material for Li metal protection. It shows high ionic conductivity (up to 10^{-3} S cm^{-1}) and low electronic conductivity ($<10^{-12}$ S cm^{-1}).[27] Furthermore, as uncovered by computation studies, Li_3N has unique thermodynamic stability against Li metal.[28,29] In the past, Li_3N has been explored as a coating; however, the grain sizes are too small (<160 nm), and their interconnection is too weak to suppress Li metal dendrites.[30,31] In this work, we develop in situ growth of a stable, mechanically strong and pinhole-free α-Li_3N crystalline film comprised of dense, large, and strongly interconnected grains directly on the truly clean Li metal surface, and present the excellent electrochemical performance of Li metal anodes with such a Li_3N protection layer.

RESULTS AND DISCUSSION

Synthesis of Pinhole-free-Li_3N Solid Electrolyte on Molten Li Metal. A pinhole-free-Li_3N solid electrolyte layer on Li metal was fabricated by utilizing the nitridation reaction between pure N_2 gas and fresh molten Li metal (Figure 2a and Movie S1). In a typical procedure, a Li metal foil was first sandwiched between two Cu foils and heated at 300 °C under mechanical pressure in Ar atmosphere, producing a Cu/Li/Cu sandwich architecture with good adhesion between the Cu foils and Li metal. After transfer to a N_2-filled glovebox, the Cu/Li/Cu sandwich was heated at 450 °C until the Li metal melted. The two Cu foils with liquid lithium between them were then pulled apart quickly, and further baked at 450 °C for 1 s to achieve the pinhole-free-Li_3N film on Li metal. Right after this, the sample was cooled down to room temperature and transferred to an Ar-filled glovebox. Rapidly pulling apart the Cu foils is important to generate truly fresh and clean liquid Li metal surfaces for reaction. Immediately upon exposure, the fresh surfaces of the liquid Li metal quickly turned black, forming a uniform crystalline Li_3N layer on the Li metal surface. The subsequent heat treatment process densified the Li_3N layer and further

DOI: 10.1021/acscentsci.7b00480
ACS Cent. Sci. 2018, 4, 97−104

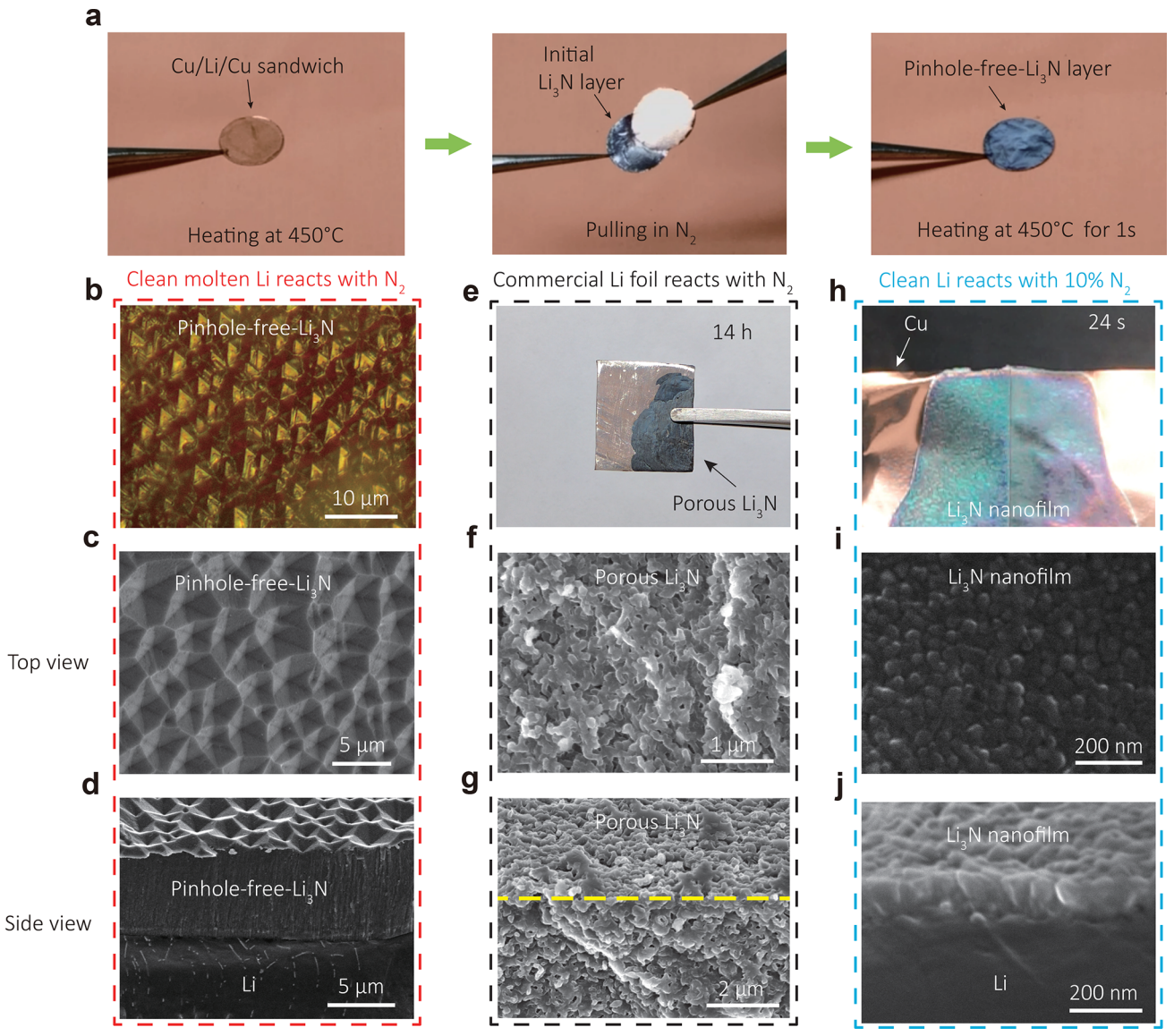

Figure 2. Fabrication and morphology of the pinhole-free-Li_3N–Li metal anode. (a) The fabrication process of the pinhole-free-Li_3N–Li metal anode. A Cu/Li/Cu sandwich was heated at 450 °C until the Li metal melted. The two Cu foils with liquid lithium on them were then separated away quickly, exposing the fresh Li metal surfaces to nitrogen gas, and further baked for 1 s. (b–d) Dark field optical (b), top-view (c), and cross-section (d) SEM images of a pinhole-free-Li_3N–Li metal anode. (e–g) Digital (e), top-view (f), and cross-section (g) SEM images of a Li metal foil with a superficial native film after being placed in a nitrogen filled glovebox for 14 h. A porous Li_3N flake was achieved after the nitridation reaction. (h–j) Digital (h), top-view (i), and cross-section (j) SEM images after the reaction between a fresh and clean Li metal surface and low-concentration N_2 gas (~10%) at room temperature. Li_3N nanofilms on the Li metal surface were observed.

improved its crystallinity. Optical and scanning electron microscope (SEM) images show that a Li_3N layer with very large grains is successfully grown on the Li metal surface (Figure 2b,c). The surface of the Li_3N layer is homogeneous and shows well-developed Li_3N crystal planes, indicating high crystallinity. Cross-section SEM images show that the Li_3N layer is comprised of strongly interconnected grains with tunable thickness from 2 to 200 μm (Figure 2d and Figure S1). The dense, pinhole-free structure and reasonable thickness of the Li_3N layer are important for implementation in batteries to prevent infiltration of liquid electrolytes and to suppress the growth of Li dendrites.

Different from any previous studies, here the two vital factors for the successful synthesis of the pinhole-free-Li_3N solid electrolyte are the creation of a truly pristine lithium surface and utilization of high reaction temperature. Because of its high reactivity, commercially obtained Li metal is always covered by a native surface film,[32] and freshly exposed Li metal surfaces cannot remain clean even in inert atmosphere due to the fast reaction between Li metal and trace amounts of active gases, such as O_2, water, and CO_2 (Figure S2). This native film leads to a nonuniform and slow (10–20 h) nitridation reaction (Figure 2e and Figure S3), where Li_3N flakes with small particle size (~200 nm) and porous structure were formed (Figure 2f,g) instead of a dense pinhole-free-Li_3N layer as shown in Figure 2c,d. To gain insight into the importance of a fresh and clean Li metal surface for the growth of a uniform Li_3N film, a Cu/Li/Cu sandwich architecture was torn apart in an argon atmosphere with a low content of N_2 gas (~10% by volume) at room temperature. Homogeneous nitridation of the fresh Li metal surface was observed, generating uniform Li_3N nanofilms with tunable thickness of 50–400 nm and corresponding color change during the reaction (Figure 2h–j, Figure S4–6 and Movie S2). The size

DOI: 10.1021/acscentsci.7b00480
ACS Cent. Sci. 2018, 4, 97–104

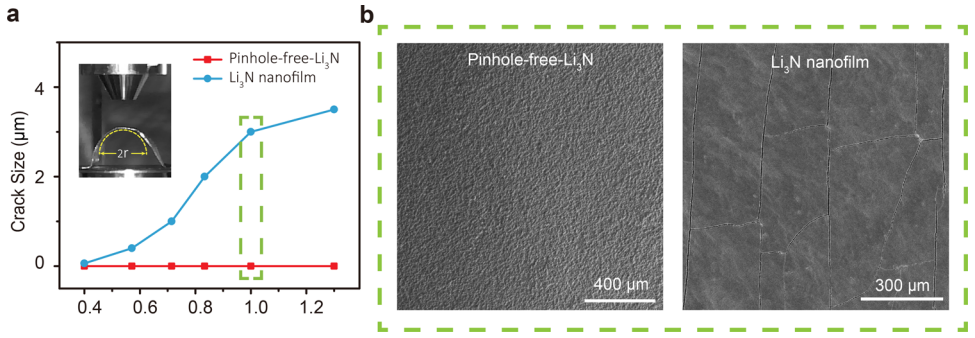

Figure 3. Mechanical properties characterizations of the pinhole-free-Li_3N–Li metal anode. (a) Crack size vs curvature plot for a pinhole-free-Li_3N film and a Li_3N nanofilm. The inset in (a) shows a digital image of a pinhole-free-Li_3N–Li metal anode under bending. (b) Top-view SEM images of a pinhole-free-Li_3N film (left) and a Li_3N nanofilm (right) under bending at a curvature radius of 1 cm.

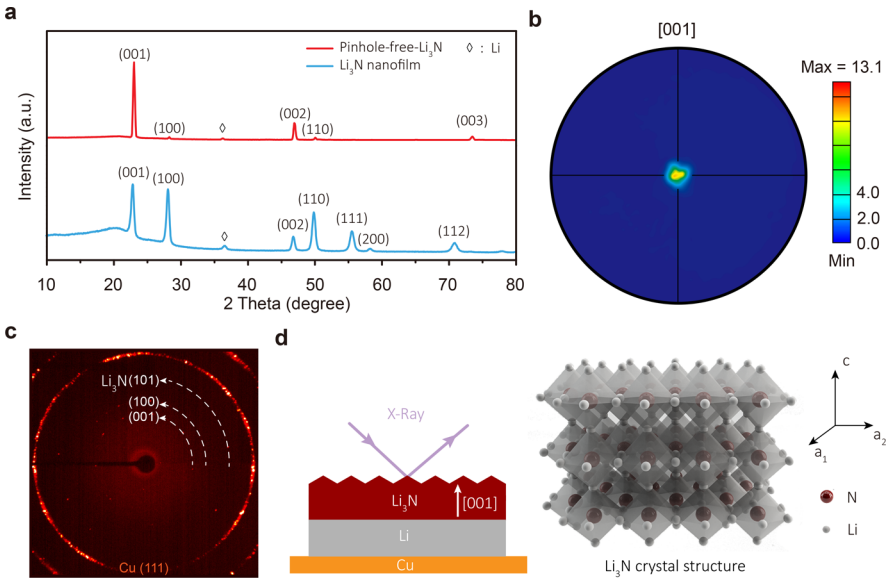

Figure 4. Structural characterizations of the pinhole-free-Li_3N–Li metal anode. (a) XRD pattern of the pinhole-free-Li_3N–Li metal anode and the Li metal anode with a Li_3N nanofilm. (b) Pole figure of the (001) plane of the dense pinhole-free-Li_3N layer. (c) 2D XRD pattern of the pinhole-free-Li_3N layer within a sample area of 100 × 100 μm. (d) Schematic of the Li metal anode with an oriented pinhole-free-Li_3N layer. XRD results indicate that the as-grown pinhole-free-Li_3N layer is highly oriented along the [001] crystalline direction and is comprised of large grains tens of micrometers in size.

of Li_3N particles for these nanofilms ranges from 50 to 100 nm (Figure 2i). Hence, using truly pristine Li metal surfaces avoids the influence of the native film and enables a fast and homogeneous nitridation reaction over the whole Li metal surface. The other key factor for the formation of a dense pinhole-free-Li_3N film with large grains is the high reaction temperature. With increased reaction temperature (100 °C, below the melting point of Li metal at 180.5 °C), a denser Li_3N nanofilm was achieved in comparison to that obtained at room temperature (Figure S7). When we further increased the reaction temperature to 450 °C, a pinhole-free-Li_3N film with large, strongly interconnected grains was achieved (Figure 2d). Therefore, the nitridation of truly pristine Li metal surface at high temperature enables the fast, uniform growth of a dense pinhole-free-Li_3N film with large grains on the Li metal surface.

Characterization of Pinhole-free-Li_3N Solid Electrolyte. One main limitation of nanofilms is their poor mechanical durability. They are prone to failure during battery fabrication and cycling processes due to the weak interconnection between the nanoparticles of the films (Figures S8 and S9). Until now, little emphasis has been placed on the development of mechanically robust protective layers for Li metal. Our pinhole-free-Li_3N film successfully achieves good mechanical durability due to the strongly interconnected large crystalline grains. The pinhole-free-Li_3N film integrated Li metal anode is flexible and pliable. Bending measurements and SEM investigation show that the pinhole-free-Li_3N layer on the Li metal surface does not fail even at a curvature radius of 0.8 cm, indicating extraordinary mechanical flexibility and durability compared to the Li_3N nanofilm (Figure 3a and Figure 3b left). For comparison, bending measurements were also carried out on a Li_3N nanofilm modified Li metal anode. The Li_3N nanofilm shows tiny cracks (~200 nm) right after its fabrication (Figure S8). Bending the Li_3N nanofilm to a curvature radius of 1 cm (Figure 3b right) generates a number of cracks with size ~3 μm, which is large enough for Li metal dendrites to grow through. Because of the higher thermal expansion coefficient of Li metal compared to that of Li_3N,[33] built-in compressive stress is produced when the pinhole-free-Li_3N–Li metal sample cools from 450 °C to room temperature after its fabrication. The compressive stress in thin film mechanics is known to counteract the tension during bending and gives rise to good mechanical robustness.[34]

DOI: 10.1021/acscentsci.7b00480
ACS Cent. Sci. 2018, 4, 97–104

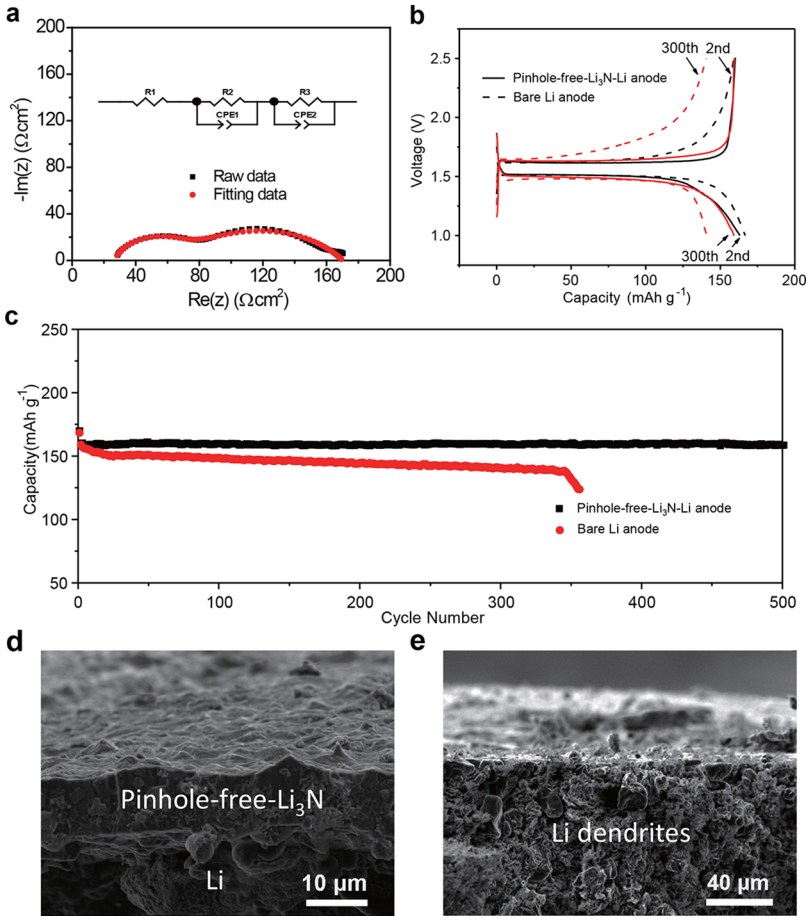

Figure 5. Electrochemical characteristics of the pinhole-free-Li_3N−Li metal anode. (a) Nyquist plots of a Li|pinhole-free-Li_3N|Li symmetric cell. The black dot line denotes the experimental data, while the red one represents the fitting data using the equivalent circuit modeling (inset of a). (b) The voltage profiles of the Li|$Li_4Ti_5O_{12}$ cells with the pinhole-free-Li_3N−Li and the bare Li metal electrodes at 1 C. (c) Cycling behaviors of the Li|$Li_4Ti_5O_{12}$ cells with the pinhole-free-Li_3N−Li and the bare Li metal electrodes at 1 C. (d, e) Cross-section SEM images of a pinhole-free-Li_3N−Li metal anode (d) and a bare Li metal anode (e) after 100 cycles.

X-ray diffraction (XRD) measurements were performed to determine the crystalline phase and grain orientation of the product (Figure 4a). The symmetrical θ-2θ scan revealed a pure α-phase of Li_3N which is corroborated by the powder diffraction file 00-30-0759 (space group: *P6/mmm*) for the pinhole-free-Li_3N. Only (001), (002), and (003) peaks are visible from the α-phase Li_3N, clearly indicating that the crystal grains of as-grown α-phase Li_3N are highly oriented along the [001] direction perpendicular to the Li substrate surface. This is quite different from the Li_3N nanofilm achieved at room temperature, which mainly exhibits random grain orientation shown in Figure 4a in blue. To fully characterize the texture of a crystalline Li_3N film, the pole figure measurements were carried out.[35] Two pole figures were acquired with the Bragg angles fixed at $2\theta = 22.96°$ and 70.99° corresponding to Li_3N (001) and Li_3N (112) crystallographic planes. The diffracted intensity was collected by varying the tilt, χ, and the rotation, ϕ, angles with respect to the normal direction of a sample surface. Figure 4b shows the Li_3N (001) pole figure from pinhole-free-Li_3N sample. As can be seen from the figure, all diffracted intensity from (001) planes is concentrated around $\chi = 0°$, confirming that crystallographic grain orientation of pinhole-free-Li_3N film is exclusively along [001] direction normal to the film's surface. As shown in Figure S10, the Li_3N (112) pole figure exhibits a ring of a constant intensity at an angle $\chi = 46.7°$ consistent with the angle between (001) and (112) planes of hexagonal Li_3N. The constant intensity of Li_3N (112) ring confirms a random in-plane orientation of the Li_3N grains. The distribution of (001) and (112) pole figure densities indicates that Li_3N film is highly textured exhibiting so-called fiber texture with grains oriented [001] out-of-plane, but having random orientation in-plane.

The size of Li_3N crystal grains can be qualitatively estimated by X-ray diffraction in transmission geometry and using X-ray source with the spot size of ~100 μm in diameter. The two-dimensional (2D) XRD pattern shows only several individual spots corresponding to Li_3N phase within a sample area of 100 × 100 μm, suggesting that the grain size of Li_3N is around few tens of micrometers (Figure 4c). Meanwhile, the highly oriented crystalline plane of Li_3N crystals also supports the large grain size of Li_3N (Figure 2c). Thus, the pinhole-free-Li_3N layer is vertically grown on the Li metal substrate along the [001] crystalline direction of hexagonal α-phase Li_3N with a large grain size (Figure 4d), in contrast to the random growth of the Li_3N nanofilm achieved at room temperature. The oriented growth and large grain size of the dense Li_3N film also support its good mechanical properties.

Good ambient stability can improve material safety and simplify requirements for use in industrial battery fabrication environments. To study the ambient stability of the pinhole-free-Li_3N−Li anode, XRD was performed after exposure to ambient

DOI: 10.1021/acscentsci.7b00480
ACS Cent. Sci. 2018, 4, 97−104

conditions to identify the formation of any new reaction products. Interestingly, although Li_3N nanofilms usually exhibit high reactivity with ambient air, the XRD pattern of the pinhole-free-Li_3N−Li metal anode shows clear Li signals and strong Li_3N signals after exposure in ambient air with 40% humidity for 8 h, indicating the good stability of the pinhole-free-Li_3N−Li metal anode in ambient conditions (Figure S11). Industrial battery fabrication is performed in a dry room with a relative humidity of less than 1% and an operating period of less than 8 h. The good ambient stability of the pinhole-free-Li_3N−Li metal anode makes it promising in industry battery applications. Our pinhole-free-Li_3N solid electrolyte layer is highly crystalline and dense, and once it is exposed to ambient air, a protective passivation layer forms on the surface and limits further reaction with the surrounding atmosphere.[27] Furthermore, SEM investigations show that there is no significant change before and after the storage of a pinhole-free-Li_3N−Li metal anode in a widely used ether-based electrolyte for 30 days, indicating its good stability and compatibility with liquid electrolytes (Figure S12).

Electrochemical Performance of Pinhole-free-Li_3N Integrated Li Metal Anode. To measure the ionic conductivity of the pinhole-free-Li_3N layer, electrochemical impedance spectroscopy (EIS) measurements were carried out on an all-solid-state Li|pinhole-free-Li_3N|Li symmetric cell (Figure 5a). Before the construction of the symmetric cell, a 50 nm thick Au layer was deposited onto a 200 μm thick pinhole-free-Li_3N film using thermal evaporation techniques to serve a buffer layer to improve the contact between the pinhole-free-Li_3N solid electrolyte and Li metal as Au and Li form an alloy at room temperature.[36,37] The first semicircle at relatively high frequency in the Nyquist plots can be used to analyze the bulk resistance of the pinhole-free-Li_3N film, while the interfacial resistance between the Li metal and pinhole-free-Li_3N layer can be calculated based on the second semicircle.[36,38] The first semicircle yields a resistance of 87 Ω cm^2, and the ionic conductivity of the pinhole-free-Li_3N film is calculated as 2.3×10^{-4} S cm^{-1}. Meanwhile, the measured ionic conductivity is as high as 5.2×10^{-4} S cm^{-1} for a 20 μm pinhole-free-Li_3N film based on symmetric cells made of either two bare Li metal electrodes or two pinhole-free-Li_3N−Li electrodes using liquid electrolytes (Figure S13). With the calculated ionic conductivity of $2-5 \times 10^{-4}$ S cm^{-1}, a 2 μm thick film will have an ionic resistance of 0.4 to 1 Ohm cm^{-2}, 10 μm thick film will have an ionic resistance of 2 to 5 Ohm cm^{-2}. These resistance values are low enough for pinhole-free-Li_3N to serve as an interfacial coating layer. Thus, one can expect fast lithium stripping/plating kinetics and stable cycling behavior of the pinhole-free-Li_3N−Li metal anode due to the excellent mechanical durability, good stability, and high ionic conductivity of the Li_3N film.

To evaluate the electrochemical stability of the pinhole-free-Li_3N−Li metal anode, we paired it with a $Li_4Ti_5O_{12}$ electrode since $Li_4Ti_5O_{12}$ has a flat discharge/charge plateau at ∼1.5 V and very stable cyclability without an increase in potential hysteresis during cycling. The surface of $Li_4Ti_5O_{12}$ particles is free of solid electrolyte interphase (SEI) film, so it does not consume organic electrolyte and active Li. Therefore, we can truly evaluate the stability of the pinhole-free-Li_3N−Li metal anode without the influence of the counter electrode. During discharge of a cell with a $Li_4Ti_5O_{12}$ counter electrode, lithium is electrochemically stripped from the Li metal anode, conducted through the pinhole-free-Li_3N layer and liquid electrolytes, and intercalated into the $Li_4Ti_5O_{12}$ counter electrode. Then, upon charging, it is extracted from the $Li_4Ti_5O_{12}$ host and deposited back on the Li anode underneath the pinhole-free-Li_3N layer. Figure S14 shows the voltage profiles of a pinhole-free-Li_3N−Li|$Li_4Ti_5O_{12}$ cell and its bare Li anode Li|$Li_4Ti_5O_{12}$ counterpart for cycling at 1 C for $Li_4Ti_5O_{12}$ (0.8 mA cm^{-2}), respectively. An in-depth comparison of voltage profiles at each labeled cycle is shown in Figure 5b and Figure S15. After activation (the first cycle), the pinhole-free-Li_3N−Li|$Li_4Ti_5O_{12}$ cell shows similar flat discharge and charge voltage plateaus (∼1.51 V and ∼1.61 V, respectively, Figure 5b) as the Li|$Li_4Ti_5O_{12}$ cell without any potential hysteresis for the second cycle. The pinhole-free-Li_3N−Li|$Li_4Ti_5O_{12}$ cell exhibits stable discharge/charge plateaus and high capacities with ∼99.99% Coulombic efficiency on cycling with a high capacity of 160 mAh g^{-1} for the second cycle and 159 mAh g^{-1} for the 500th cycle (Figure 5b,c and Figure S16). In contrast, the Li|$Li_4Ti_5O_{12}$ cell displays obviously increased potential polarization and capacity decay on cycling. Its capacity decays from 159 mAh g^{-1} for the second cycle to 138 mAh g^{-1} for the 340th cycle, which quickly drops down to 132 mAh g^{-1} for the 350th cycle (Figure 5c). Additionally, the Li|$Li_4Ti_5O_{12}$ cell using Li_3N nanofilm coated Li metal anode shows better electrochemical stability than that of the bare Li|$Li_4Ti_5O_{12}$ cell but worse than the pinhole-free-Li_3N−Li|$Li_4Ti_5O_{12}$ cell during cycling due to the weak interconnection between the Li_3N nanoparticles and cracking of the nanofilms (Figure S17). Thus, compared with the Li_3N nanofilm for Li metal anode protection, this pinhole-free-Li_3N material shows much better protection in terms of suppression of Li metal dendrite growth and improved battery cycling. Meanwhile, the pinhole-free-Li_3N−Li|$Li_4Ti_5O_{12}$ cells shows excellent rate capability with 69% of the 0.2 C (0.19 mA cm^{-2}) capacity at 6 C (5.59 mA cm^{-2}) due to the good ionic conductivity of the Li_3N layer on the Li metal surface (Figure S18). The morphology and structure of the pinhole-free-Li_3N−Li metal anode was observed after 100 cycles. The pinhole-free-Li_3N layer preserves its structural integrity over battery cycling, suggesting that stable Li_3N-liquid electrolyte and Li metal-Li_3N interfaces are achieved for the cells with the pinhole-free-Li_3N−Li metal anode, providing good protection of the Li metal anode and enabling good battery performance (Figure 5d). In comparison, the bare lithium metal anode has a loose and porous structure with randomly grown dendrites after 100 discharge/charge cycles, suggesting serious corrosion of the anode (Figure 5e). The accumulation of SEI and "dead lithium" at the bare Li metal anode hurts the kinetics of the control cell, which, combined with the consumption of liquid electrolytes, eventually leads to the failure of the battery.

CONCLUSIONS

In summary, we have fabricated a robust pinhole-free-Li_3N solid electrolyte film with large, strongly interconnected grains on Li metal surface through the reaction between clean molten lithium foil and pure nitrogen gas. The pinhole-free-Li_3N layer bonds strongly to Li metal with oriented growth of dense α-Li_3N crystals along the [001] direction. The Li_3N coating exhibits excellent mechanical durability, high ionic conductivity, and high electrochemical stability with liquid electrolytes. By restraining the growth of lithium dendrites, suppressing parasitic side reactions, and minimizing the interfacial resistance between the solid electrolyte and Li metal, the pinhole-free-Li_3N film therefore significantly improves the electrochemical plating and stripping behavior of Li metal. Our work demonstrates that a pinhole-free-Li_3N film with large and strongly interconnected grains, and high ionic conductivity opens new prospects to

DOI: 10.1021/acscentsci.7b00480
ACS Cent. Sci. 2018, 4, 97−104

address the challenges that high-energy-density lithium batteries face.

METHODS

Materials Synthesis. To fabricate a Cu/Li/Cu sandwich, a Li metal foil (99.9%, Alfa Aesar) was first sandwiched between two Cu foils and then heated on a hot plate at 300 °C in an Ar-filled glovebox with moisture level and oxygen level below 0.1 ppm. Once the Li metal melted, a flat aluminum block was pressed on the top Cu foil, and good adhesion between Li metal and Cu foils was achieved. During this process, 500 μm thick Si slides were sandwiched between two Cu foil sheets as spacers to control the thickness of the final Li layer inside Cu/Li/Cu sandwich structure as 500 μm. To prepare Li_3N nanofilm modified Li metal, a small amount of N_2 gas (~10% by volume) was introduced into the pure Ar atmosphere. The cooled Cu/Li/Cu sandwich architecture was quickly torn apart into two pieces of Cu-foil supported Li metal. The nitridation reaction took place immediately after the exposure of the fresh Li metal surface, producing a Li_3N nanofilm on the Li metal surface. To obtain Li_3N nanofilms with certain thickness, the nitridation reaction was terminated by flowing pure argon gas. Pinhole-free-Li_3N -Li metal anodes were prepared by a similar procedure in a pure N_2-filled glovebox. The Cu/Li/Cu sandwich architecture was heated at 450 °C until the Li metal melted. The two Cu foils with liquid lithium on them were then separated away quickly and further baked for 1 s to form pinhole-free-Li_3N−Li metal anodes. After the reaction, the as-prepared anodes were stored in an Ar atmosphere to avoid further nitridation reactions. For comparison, the Li metal control sample was prepared using the same method by pulling apart Cu/Li/Cu sandwich structures at 450 °C, except that the whole process was done in an Ar atmosphere. Samples with the thickness between 250−300 μm were chosen for further mechanical and electrochemical tests.

Characterization. The morphology of the samples was characterized using a FEI XL30 Sirion scanning electron microscope. Electrodes after electrochemical cycling were rinsed in 1,3-dioxolane (DOL) and dried in an argon-filled glovebox before their SEM investigation. All the samples for SEM were sealed in Ar before being transferred into the SEM chamber. The X-ray diffraction measurements were carried out employing Panalytical X'Pert Material Research diffractometer with Cu Kα radiation (λ = 1.5419 Å). In order to protect specimens from the environmental degradation, the samples were sealed with Kapton tape before conducting X-ray diffraction experiments. The pole figure measurements were performed using X-ray lens delivering a point-focus X-ray beam. The beam size was controlled by a cross-slit collimator. During the prolonged pole figure measurements, the samples were additionally sealed inside the Anton-Paar stage with continuous flow of Ar gas.

Electrochemical Measurements. Battery performance was evaluated by galvanostatic cycling of 2032-type coin cells (MTI Corporation) on a LAND 8-channel battery tester. The electrodes used were pinhole-free-Li_3N−Li metal foils or freshly scraped Li metal foils (99.9%, Alfa Aesar). $Li_4Ti_5O_{12}$ electrodes were used as the counter electrodes. Ether-based electrolyte with lithium bis(trifluoromethanesulphonyl)imide (LiTFSI) and carbonate-based electrolyte with $LiPF_6$ are two widely used electrolytes for Li metal anode studies. In our work, ether-based electrolyte with LiTFSI was used for the electrochemical characterization. The cells were assembled in an argon-filled glovebox using 1 M LiTFSI in a mixture of 1,3-dioxolane/1,2-dimethoxyethane (DME) (1:1 v/v) with 1 wt % lithium nitrate as the electrolyte and a Celgard 2325 membrane as the separator. $Li_4Ti_5O_{12}$ electrodes were constructed using a slurry method by mixing commercial $Li_4Ti_5O_{12}$ powder, carbon black and polyvinylidene fluoride (PVDF) binder in the weight ratio of 90:5:5 in *N*-methyl-2-pyrrolidinone (NMP) solvent. The typical mass loading of the $Li_4Ti_5O_{12}$ electrodes was ~5 mg cm^{-2}. The cutoff potential range for pinhole-free-Li_3N−Li|$Li_4Ti_5O_{12}$ and Li|$Li_4Ti_5O_{12}$ cells is 1−2.5 V. A Biologic VMP3 system was employed to carry out the electrochemical impedance spectroscopy measurements. To fabricate an all-solid-state Li|pinhole-free-Li_3N|Li symmetric cell, a pinhole-free-Li_3N/Li/Cu structure with a ~ 200 μm pinhole-free-Li_3N layer bonded on a ~ 50 μm lithium layer was first prepared by tearing apart a Cu/Li/Cu sandwich architecture at 450 °C in pure N_2 atmosphere. Then a 50 nm thick Au layer was deposited on top of the pinhole-free-Li_3N layer using thermal evaporation techniques. Finally, the all-solid-state Li|pinhole-free-Li_3N|Li symmetric cell was assembled by covering the Au deposited pinhole-free-Li_3N/Li structure with a 50 μm thick lithium metal foil. The cell was heated at 80 °C for 1 h to improve the interface contact between the lithium foil and the pinhole-free-Li_3N electrolyte.

ASSOCIATED CONTENT

Supporting Information

The Supporting Information is available free of charge on the ACS Publications website at DOI: 10.1021/acscentsci.7b00480.

Figures S1−S18 (PDF)

Movies S1 and S2 (AVI1, AVI2)

AUTHOR INFORMATION

Corresponding Author

*E-mail: yicui@stanford.edu.

ORCID

Yanbin Li: 0000-0002-5285-8602

Allen Pei: 0000-0001-8930-2125

Yuzhang Li: 0000-0002-1502-7869

Guangyuan Zheng: 0000-0003-0286-5908

Yi Cui: 0000-0002-6103-6352

Author Contributions

#Y.L. and Y.S. contributed equally to this work.

Notes

The authors declare no competing financial interest.

ACKNOWLEDGMENTS

Y.C. acknowledges the support from the Assistant Secretary for Energy Efficiency and Renewable Energy, Office of Vehicle Technologies of the U.S. Department of Energy under the Advanced Battery Materials Research (BMR) Program and Battery500 Consortium. A.P. acknowledges support by the Department of Defense (DoD) through the National Defense Science & Engineering Graduate Fellowship (NDSEG) Program and support by the Stanford Graduate Fellowship. Mr. Qiran Xiao (Department of Materials Science and Engineering, Stanford University) is acknowledged for helpful discussion in mechanical properties analysis. Part of this work was performed at the Stanford Nano Shared Facilities (SNSF).

REFERENCES

(1) Armand, M.; Tarascon, J.-M. Building better batteries. *Nature* **2008**, *451*, 652−657.

DOI: 10.1021/acscentsci.7b00480
ACS Cent. Sci. 2018, 4, 97−104

(2) Bruce, P. G.; Freunberger, S. A.; Hardwick, L. J.; Tarascon, J.-M. Li-O_2 and Li-S batteries with high energy storage. *Nat. Mater.* **2012**, *11*, 19−29.
(3) Sun, Y.; Liu, N.; Cui, Y. Promises and challenges of nanomaterials for lithium-based rechargeable batteries. *Nature Energy* **2016**, *1*, 16071.
(4) Kim, H.; Jeong, G.; Kim, Y.-U.; Kim, J. -H; Park, C.-M.; Sohn, H.-J. Metallic anodes for next generation secondary batteries. *Chem. Soc. Rev.* **2013**, *42*, 9011−9034.
(5) Peled, E. The electrochemical behavior of alkali and alkaline earth metals in nonaqueous battery systems-The solid electrolyte interphase model. *J. Electrochem. Soc.* **1979**, *126*, 2047−2051.
(6) Xu, W.; Wang, J.; Ding, F.; Chen, X.; Nasybulin, E.; Zhang, Y.; Zhang, J.-G. Lithium metal anodes for rechargeable batteries. *Energy Environ. Sci.* **2014**, *7*, 513−537.
(7) Rosso, M.; Brissot, C.; Teyssot, A.; Dolle, M.; Sannier, L.; Tarascon, J.-M.; Bouchet, R.; Lascaud, S. Dendrite short-circuit and fuse effect on Li/polymer/Li cells. *Electrochim. Acta* **2006**, *51*, 5334−5340.
(8) Tikekar, M. D.; Choudhury, S.; Tu, Z.; Archer, L. A. Design principles for electrolytes and interfaces for stable lithium-metal batteries. *Nature Energy* **2016**, *1*, 16114.
(9) Yoshimatsu, I.; Hirai, T.; Yamaki, J. -i. Lithium electrode morphology during cycling in lithium cells. *J. Electrochem. Soc.* **1988**, *135*, 2422−2427.
(10) Yamaki, J.-i.; Tobishima, S.-I; Hayashi, K.; Saito, K.; Nemoto, Y.; Arakawa, M. A consideration of the morphology of electrochemically deposited lithium in an organic electrolyte. *J. Power Sources* **1998**, *74*, 219−227.
(11) Harry, K. J.; Hallinan, D. T.; Parkinson, D. Y.; MacDowell, A. A.; Balsara, N. P. Detection of subsurface structures underneath dendrites formed on cycled lithium metal electrodes. *Nat. Mater.* **2014**, *13*, 69−73.
(12) Chandrashekar, S.; Trease, N. M.; Chang, H. J.; Du, L.-S.; Grey, C. P.; Jerschow, A. 7Li MRI of Li batteries reveals location of microstructural lithium. *Nat. Mater.* **2012**, *11*, 311−315.
(13) Bhattacharyya, R.; Key, B.; Chen, H.; Best, A. S.; Hollenkamp, A. F.; Grey, C. P. In situ NMR observation of the formation of metallic lithium microstructures in lithium batteries. *Nat. Mater.* **2010**, *9*, 504−510.
(14) Gireaud, L.; Grugeon, S.; Laruelle, S.; Yrieix, B.; Tarascon, J.-M. Lithium metal stripping/plating mechanisms studies: A metallurgical approach. *Electrochem. Commun.* **2006**, *8*, 1639−1649.
(15) Ding, F.; Xu, W.; Graff, G. L.; Zhang, J.; Sushko, M. L.; Chen, X.; Shao, Y.; Engelhard, M. H.; Nie, Z.; Xiao, J.; Liu, X.; Sushko, P. V.; Liu, J.; Zhang, J.-G. Dendrite-free lithium deposition via self-healing electrostatic shield mechanism. *J. Am. Chem. Soc.* **2013**, *135*, 4450−4456.
(16) Ota, H.; Shima, K.; Ue, M.; Yamaki, J.-i. Effect of vinylene carbonate as additive to electrolyte for lithium metal anode. *Electrochim. Acta* **2004**, *49*, 565−572.
(17) Li, W.; Yao, H.; Yan, K.; Zheng, G.; Liang, Z.; Chiang, Y.-M.; Cui, Y. The synergetic effect of lithium polysulfide and lithium nitrate to prevent lithium dendrite growth. *Nat. Commun.* **2015**, *6*, 7436.
(18) Kozen, A. C.; Lin, C.-F.; Pearse, A. J.; Schroeder, M. A.; Han, X.; Hu, L.; Lee, S.-B.; Rubloff, G. W.; Noked, M. Next-generation lithium metal anode engineering via atomic layer deposition. *ACS Nano* **2015**, *9*, 5884−5892.
(19) Yan, K.; Lee, H.-W.; Gao, T.; Zheng, G.; Yao, H.; Wang, H.; Lu, Z.; Zhou, Y.; Liang, Z.; Liu, Z.; Chu, S.; Cui, Y. Ultrathin two-dimensional atomic crystals as stable interfacial layer for improvement of lithium metal anode. *Nano Lett.* **2014**, *14*, 6016−6022.
(20) Zheng, G.; Lee, S. W.; Liang, Z.; Lee, H.-W.; Yan, K.; Yao, H.; Wang, H.; Li, W.; Chu, S.; Cui, Y. Interconnected hollow carbon nanospheres for stable lithium metal anodes. *Nat. Nanotechnol.* **2014**, *9*, 618−623.
(21) Lin, D.; Liu, Y.; Chen, W.; Zhou, G.; Liu, K.; Dunn, B.; Cui, Y. Conformal lithium fluoride protection layer on three-dimensional lithium by nonhazardous gaseous reagent freon. *Nano Lett.* **2017**, *17*, 3731−3737.
(22) Gao, Y.; Zhao, Y.; Li, Y. C.; Huang, Q.; Mallouk, T. E.; Wang, D. Interfacial chemistry regulation via a skin-grafting strategy enables high-performance lithium-metal batteries. *J. Am. Chem. Soc.* **2017**, *139*, 15288−15291.
(23) Li, N.-W.; Yin, Y.-X.; Yang, C.-P.; Guo, Y.-G. An artificial solid electrolyte interphase layer for stable lithium metal anodes. *Adv. Mater.* **2016**, *28*, 1853−1858.
(24) Yan, K.; Lu, Z.; Lee, H.-W.; Xiong, F.; Hsu, P.-C.; Li, Y.; Zhao, J.; Chu, S.; Cui, Y. Selective deposition and stable encapsulation of lithium through heterogeneous seeded growth. *Nature Energy* **2016**, *1*, 16010.
(25) Lin, D.; Liu, Y.; Liang, Z.; Lee, H.-W.; Sun, J.; Wang, H.; Yan, K.; Xie, J.; Cui, Y. Layered reduced graphene oxide with nanoscale interlayer gaps as a stable host for lithium metal anodes. *Nat. Nanotechnol.* **2016**, *11*, 626−632.
(26) Liang, Z.; Lin, D.; Zhao, J.; Lu, Z.; Liu, Y.; Liu, C.; Lu, Y.; Wang, H.; Yan, K.; Tao, X.; Cui, Y. Composite lithium metal anode by melt infusion of lithium into a 3D conducting scaffold with lithiophilic coating. *Proc. Natl. Acad. Sci. U. S. A.* **2016**, *113*, 2862−2867.
(27) Alpen, U. v. Li_3N: A promising Li ionic conductor. *J. Solid State Chem.* **1979**, *29*, 379−392.
(28) Zhu, Y.; He, X.; Mo, Y. Origin of outstanding stability in the lithium solid electrolyte materials: Insights from thermodynamic analyses based on first-principles calculations. *ACS Appl. Mater. Interfaces* **2015**, *7*, 23685−23693.
(29) Zhu, Y.; He, X.; Mo, Y. Strategies based on nitride materials chemistry to stabilize Li metal anode. *Adv. Sci.* **2017**, *4*, 1600517.
(30) Wu, M.; Wen, Z.; Liu, Y.; Wang, X.; Huang, L. Electrochemical behaviors of a Li_3N modified Li metal electrode in secondary lithium batteries. *J. Power Sources* **2011**, *196*, 8091−8097.
(31) Ma, G.; Wen, Z.; Wu, M.; Shen, C.; Wang, Q.; Jin, J.; Wu, X. A lithium anode protection guided highly-stable lithium-sulfur battery. *Chem. Commun.* **2014**, *50*, 14209−14212.
(32) Kanamura, K.; Tamura, H.; Shiraishi, S.; Takehara, Z.-I. XPS analysis for the lithium surface immersed in γ-butyrolactone containing various salts. *Electrochim. Acta* **1995**, *40*, 913−921.
(33) Nguyen, M. C.; Hoang, K.; Wang, C.-Z.; Ho, K.-M. Stabilities and defect-mediated lithium-ion conduction in a ground state cubic Li_3N structure. *Phys. Chem. Chem. Phys.* **2016**, *18*, 4185−4190.
(34) Bhargava, A. K.; Sharma, C. P. *Mechanical Behaviour and Testing of Materials*; PHI Learning Pvt. Ltd: New Delhi, 2011.
(35) Bunge, H.-J. *Texture Analysis in Materials Science: Mathematical Methods*; Elsevier: Butterworths, London, 2013.
(36) Tsai, C.-L.; et al. $Li_7La_3Zr_2O_{12}$ interface modification for Li dendrite prevention. *ACS Appl. Mater. Interfaces* **2016**, *8*, 10617−10626.
(37) Yuan, L.; et al. Mesoporous gold as anode material for lithium-ion cells. *J. New Mater. Electrochem. Syst.* **2007**, *10*, 95−97.
(38) Liu, T.; Ren, Y.; Shen, Y.; Zhao, S.-X.; Lin, Y.; Nan, C.-W. Achieving high capacity in bulk-type solid-state lithium ion battery based on $Li_{6.75}$ La_3 $Zr_{1.75}Ta_{0.25}O_{12}$ electrolyte: Interfacial resistance. *J. Power Sources* **2016**, *324*, 349−357.

DOI: 10.1021/acscentsci.7b00480
ACS Cent. Sci. 2018, 4, 97−104